ARCHIVES OF MECHANICS
Arch. Mech. **73** (5–6), 541–555, 2021, DOI: 10.24423/aom.3843

Uniform field within a non-elliptical inhomogeneity in the vicinity of a nearby non-circular Eshelby inclusion

X. WANG[1)], P. SCHIAVONE[2)]

[1)] *School of Mechanical and Power Engineering, East China University of Science and Technology, 130 Meilong Road, Shanghai 200237, China, e-mail: xuwang@ecust.edu.cn*

[2)] *Department of Mechanical Engineering, University of Alberta, 10-203 Donadeo Innovation Centre for Engineering, Edmonton, Alberta Canada T6G 1H9, e-mail: p.schiavone@ualberta.ca*

We rigorously prove that a non-elliptical inhomogeneity continues to permit an internal uniform stress field despite the presence of a nearby non-circular Eshelby inclusion undergoing uniform anti-plane eigenstrains when the surrounding matrix is subjected to uniform remote anti-plane stresses. Here, we adopt a specific representation of the non-circular Eshelby inclusion as a Booth's lemniscate inclusion. Our analysis indicates that the internal uniform stress field inside the non-elliptical inhomogeneity is independent of the existence of the Booth's lemniscate inclusion whereas the non-elliptical shape of the inhomogeneity is attributed entirely to its presence. Representative numerical examples are presented to demonstrate the feasibility of the proposed method of general solution.

Key words: non-elliptical inhomogeneity, Booth's lemniscate inclusion, uniform field, conformal mapping, anti-plane elasticity, inverse problem.

1. Introduction

Eshelby's uniformity property describing the stresses and strains inside elastic inhomogeneities has become and will certainly continue to be an intriguing research topic in the field of micromechanics of composites. Studies in this area are pervasive throughout the literature. For earlier contributions, interested readers are referred to a comprehensive and detailed review by Zhou *et al.* [1]. More recent studies on Eshelby's uniformity property can be found in, for example, Dai *et al.* [2, 3], Wang *et al.* [4], Wang and Schiavone [5], Wang *et al.* [6, 7], Antipov [8, 9], Marshall [10], Lim and Milton [11].

Wang *et al.* [4] and Wang and Schiavone [5] recently have established that an uncoated or coated non-elliptical inhomogeneity embedded in a matrix subjected to uniform remote anti-plane stresses will continue to admit an internal uniform stress field despite the presence of a nearby circular Eshelby inclusion undergoing uniform anti-plane eigenstrains. In practice, however, the shape of the

Eshelby inclusion need not be circular and may take on a range of complex shapes ranging from elliptical, hypotrochidal, rectangular to polygonal and polyhedral [12–14]. It is therefore of interest to ask whether the uniformity property inside the inhomogeneity can be maintained when the nearby Eshelby inclusion has a non-circular shape? This is the question we address in this paper.

We consider the internal stress state inside a non-elliptical elastic inhomogeneity interacting with a non-circular Eshelby inclusion when the surrounding matrix is subjected to uniform remote stresses in anti-plane shear. The non-circular inclusion undergoing uniform anti-plane eigenstrains is represented by a Booth's lemniscate. Our objective is to maintain a state of uniform stress state inside the inhomogeneity by carefully designing the non-elliptical shape of the inhomogeneity given the presence of the nearby Booth's lemniscate inclusion. Using analytic continuation, the analytic function originally defined in the matrix is extended to the domain occupied by the Booth's lemniscate inclusion in which it possesses two first-order poles. Consequently, the presence of the Booth's lemniscate inclusion can be conveniently incorporated into the established mapping function via the additional two first-order poles located within the unit circle in the image plane. Our analysis indicates that the uniform stress field inside the inhomogeneity is unaffected by the existence of the Booth's lemniscate inclusion whereas the non-elliptical shape of the inhomogeneity is attributed solely to its presence. In addition, the non-uniform stress field in the matrix can be determined in a straightforward manner but the non-uniform stresses within the Booth's lemniscate inclusion are more difficult to calculate since they involve the complete specification of an auxiliary function. It is expected that the present solution will find application in the optimum design of composites in which elimination of stress peaks within the elastic inhomogeneity is an essential design criterion.

2. Complex variable formulation in anti-plane elasticity

We first establish a Cartesian coordinate system $\{x_i\}$ $(i = 1, 2, 3)$. In the anti-plane shear deformations of an isotropic elastic material, the two shear stress components σ_{31} and σ_{32}, the out-of-plane displacement w and the single stress function ϕ can be expressed in terms of a single analytic function $f(z)$ of the complex variable $z = x_1 + \mathrm{i}x_2$ as [15]

$$\sigma_{32} + \mathrm{i}\sigma_{31} = \mu f'(z), \qquad \phi + \mathrm{i}\mu w = \mu f(z), \tag{2.1}$$

where μ is the shear modulus, and the two stress components can be expressed in terms of the single stress function as [15]

$$\sigma_{32} = \phi_{,1}, \qquad \sigma_{31} = -\phi_{,2}. \tag{2.2}$$

3. General solution of the inverse problem in anti-plane elasticity

As shown in Fig. 1, we consider a domain in $\Re^2$, infinite in extent, containing both a non-elliptical elastic inhomogeneity and a non-circular Eshelby inclusion undergoing uniform stress-free anti-plane eigenstrains $(\varepsilon_{31}^*, \varepsilon_{32}^*)$. The shear modulus of the elastic inhomogeneity differs from that of the matrix while the Eshelby inclusion and the matrix are assumed to have the same shear modulus. Let S_1, S_2 and S_3 denote the inhomogeneity, the matrix and the Eshelby inclusion, respectively, all of which are perfectly bonded across the inhomogeneity-matrix interface L_1 and the inclusion-matrix interface L_2. Throughout the paper, the subscripts 1, 2 and 3 are used to identify the respective quantities in S_1, S_2 and S_3.

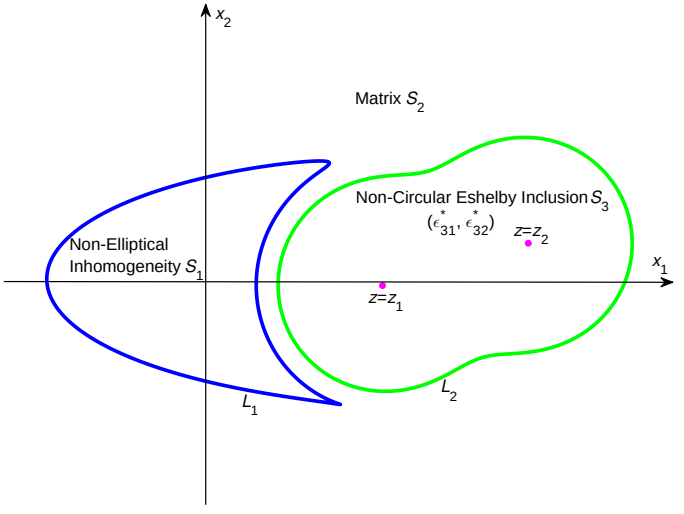

FIG. 1. A non-circular Eshelby inclusion with uniform anti-plane eigenstrains interacting with a non-elliptical inhomogeneity permitting an internal uniform stress field under uniform remote anti-plane stresses. Here the non-circular inclusion is represented by a Booth's lemniscate inclusion.

The boundary value problem for the three-phase composite takes the following form in the physical z-plane:

$$\begin{aligned} &f_2(z)+\overline{f_2(z)} = \Gamma f_1(z)+\Gamma\overline{f_1(z)}, \\ &f_2(z)-\overline{f_2(z)} = f_1(z)-\overline{f_1(z)}, \quad z\in L_1; \end{aligned} \tag{3.1a}$$

$$\begin{aligned} &f_2(z)+\overline{f_2(z)} = f_3(z)+\overline{f_3(z)}, \\ &f_2(z)-\overline{f_2(z)} = f_3(z)-\overline{f_3(z)}+2(\varepsilon_{32}^*+\mathrm{i}\varepsilon_{31}^*)z-2(\varepsilon_{32}^*-\mathrm{i}\varepsilon_{31}^*)\bar{z}, \quad z\in L_2; \end{aligned} \tag{3.1b}$$

$$f_2(z)\cong\frac{\sigma_{32}^\infty+\mathrm{i}\sigma_{31}^\infty}{\mu_2}z+O(1), \quad |z|\to\infty, \tag{3.1c}$$

where $\Gamma = \mu_1/\mu_2$. Equation (3.1a) represents the continuity of traction and displacement across the perfect inhomogeneity-matrix interface L_1; Eq. (3.1b) describes the continuity of traction and total displacement across the perfect inclusion-matrix interface L_2; Eq. (3.1c) gives the asymptotic behavior of $f_2(z)$ at infinity due to the prescribed uniform remote stresses.

Adding the two equations in Eq. (3.1b), we obtain the following condition on the interface L_2

$$f_2(z) = f_3(z) + (\varepsilon_{32}^* + \mathrm{i}\varepsilon_{31}^*)z - (\varepsilon_{32}^* - \mathrm{i}\varepsilon_{31}^*)\bar{z}, \quad z \in L_2. \tag{3.2}$$

In this paper, the non-circular Eshelby inclusion is specifically represented by a Booth's lemniscate inclusion described by

$$z = m(\xi) = c + \frac{a\mathrm{e}^{\mathrm{i}\theta}\xi}{1 - b\xi^2}, \quad \xi = m^{-1}(z),\ a > 0,\ 0 < b < 1,\ |\xi| \le 1, \tag{3.3}$$

where c is an arbitrary complex number characterizing the center of the inclusion, and θ is a phase angle characterizing inclination of the inclusion with respect to the x_1-axis.

Along the inclusion-matrix interface L_2, we have

$$\bar{z} = \bar{m}\left(\frac{1}{\xi}\right) = \bar{c} + \frac{a\mathrm{e}^{-\mathrm{i}\theta}\xi}{\xi^2 - b}, \quad |\xi| = 1. \tag{3.4}$$

Thus, an auxiliary function $D(z)$ can be constructed as follows

$$D(z) = \bar{m}\left(\frac{1}{m^{-1}(z)}\right) = \bar{c} + \frac{a\mathrm{e}^{-\mathrm{i}\theta}m^{-1}(z)}{[m^{-1}(z)]^2 - b}. \tag{3.5}$$

We can see from Eq. (3.5) that the auxiliary function $D(z)$ is analytic in the interior of the boundary L_2 except at the two points $z = z_1$ and $z = z_2$ (illustrated in Fig. 1) defined by

$$z_1 = c + \mathrm{e}^{\mathrm{i}\theta}x_0, \quad z_2 = c - \mathrm{e}^{\mathrm{i}\theta}x_0, \quad x_0 = \frac{a\sqrt{b}}{1 - b^2}, \tag{3.6}$$

at which $D(z)$ exhibits the following singular asymptotic behavior

$$\begin{aligned} D(z) &\cong \frac{a^2(1+b^2)}{2(1-b^2)^2}\frac{1}{z - z_1} + O(1), \quad z \to z_1, \\ D(z) &\cong \frac{a^2(1+b^2)}{2(1-b^2)^2}\frac{1}{z - z_2} + O(1), \quad z \to z_2. \end{aligned} \tag{3.7}$$

By considering Eqs. (3.2), (3.4) and (3.5), the analytic function $f_2(z)$ originally defined in S_2 can be extended to $S_2 \cup S_3$ in such a way that

$$f_2(z) = \begin{cases} f_2(z), & z \in S_2, \\ f_3(z) + (\varepsilon^*_{32} + \mathrm{i}\varepsilon^*_{31})z - (\varepsilon^*_{32} - \mathrm{i}\varepsilon^*_{31})D(z), & z \in S_3. \end{cases} \tag{3.8}$$

Via the analytic continuation in Eq. (3.8), $f_2(z)$ is analytic in $S_2 \cup S_3$ except at $z = \infty$ where its asymptotic behavior is given by Eq. (3.1c), and except at the two points at $z = z_1$ and $z = z_2$ where its singular or principal part denoted by $f_{2s}(z)$ is given by

$$f_{2s}(z) = -\frac{a^2(1+b^2)(\varepsilon^*_{32} - \mathrm{i}\varepsilon^*_{31})}{2(1-b^2)^2}\left(\frac{1}{z-z_1} + \frac{1}{z-z_2}\right). \tag{3.9}$$

The above indicates that $f_2(z)$ has two first-order poles at $z = z_1$ and $z = z_2$ in its extended domain S_3. Now we introduce the following conformal mapping function for the simply-connected domain occupied by the matrix and Booth's lemniscate inclusion

$$z = \omega(\xi) = R\left(\xi + \frac{p}{\xi} + \frac{q_1}{\xi - \bar{\xi}_1^{-1}} + \frac{q_2}{\xi - \bar{\xi}_2^{-1}}\right), \quad \xi = \omega^{-1}(z), \quad |\xi| \geq 1, \tag{3.10}$$

where R is a real scaling constant and p, q_1, q_2 are three complex constants. In order to ensure that the mapping in Eq. (3.10) is one-to-one outside the interface L_1, it is necessary that $\omega'(\xi) \neq 0$ for $|\xi| > 1$.

As shown in Fig. 2, using the mapping function in Eq. (3.10), the exterior of the non-elliptical inhomogeneity is mapped onto the exterior of the unit circle in the ξ-plane; the inhomogeneity-matrix interface L_1 is mapped onto the unit circle $|\xi| = 1$; the point $z = z_1$ is mapped onto the point $\xi = \xi_1 = \omega^{-1}(z_1)$, and the point $z = z_2$ is mapped onto the point $\xi = \xi_2 = \omega^{-1}(z_2)$. Thus, the presence of the non-circular Booth's lemniscate inclusion is incorporated in the mapping function through the additional two first-order poles at $\xi = \bar{\xi}_1^{-1}$, $\bar{\xi}_2^{-1}$ inside the unit circle.

In order to ensure that the stress field inside the non-elliptical inhomogeneity is uniform, $f_1(z)$ defined in the inhomogeneity should take the following form

$$f_1(z) = kz, \quad z \in S_1, \tag{3.11}$$

where k is a complex constant to be determined.

By enforcing the interface conditions in Eq. (3.1a) with the use of Eq. (3.11), we arrive at

$$f_2(\xi) = f_2(\omega(\xi)) = \frac{k(\Gamma+1)}{2}\omega(\xi) + \frac{\bar{k}(\Gamma-1)}{2}\bar{\omega}\left(\frac{1}{\xi}\right), \quad |\xi| \geq 1, \tag{3.12}$$

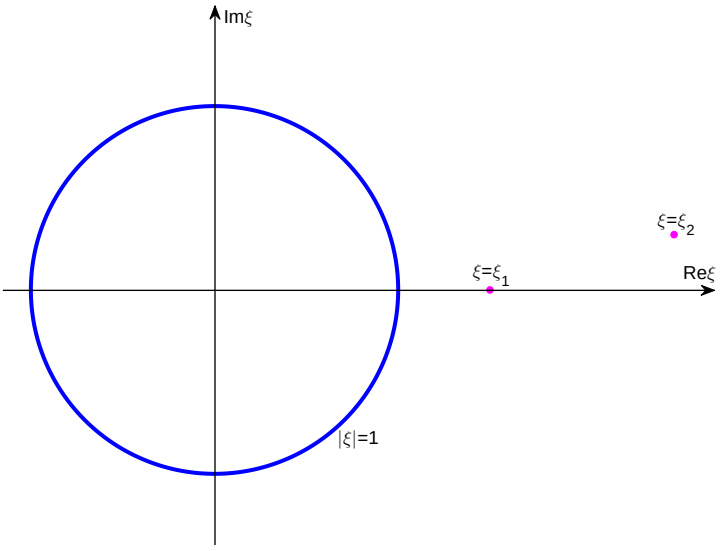

FIG. 2. The image ξ-plane.

or more explicitly

$$f_2(\xi) = \frac{Rk(\Gamma+1)}{2}\left(\xi + \frac{p}{\xi} + \frac{q_1}{\xi - \bar{\xi}_1^{-1}} + \frac{q_2}{\xi - \bar{\xi}_2^{-1}}\right) + \frac{R\bar{k}(\Gamma-1)}{2}\left(\frac{1}{\xi} + \bar{p}\xi + \frac{\bar{q}_1}{\xi^{-1} - \xi_1^{-1}} + \frac{\bar{q}_2}{\xi^{-1} - \xi_2^{-1}}\right), \quad |\xi| \geq 1. \tag{3.13}$$

Using Eq. (3.13) to satisfy the remote asymptotic behavior in Eq. (3.1c) and the presence of the two first-order poles at $z = z_1$ and $z = z_2$ in Eq. (3.9), we arrive at the following relationships:

$$\begin{aligned} &\frac{\Gamma+1}{2}k + \frac{\bar{p}(\Gamma-1)}{2}\bar{k} = \frac{\sigma_{32}^{\infty} + \mathrm{i}\sigma_{31}^{\infty}}{\mu_2}, \\ &q_1 = \frac{a^2(1+b^2)(\varepsilon_{32}^{*} + \mathrm{i}\varepsilon_{31}^{*})}{Rk(\Gamma-1)(1-b^2)^2}\frac{1}{\overline{\xi_1^2\omega'(\xi_1)}}, \\ &q_2 = \frac{a^2(1+b^2)(\varepsilon_{32}^{*} + \mathrm{i}\varepsilon_{31}^{*})}{Rk(\Gamma-1)(1-b^2)^2}\frac{1}{\overline{\xi_2^2\omega'(\xi_2)}}. \end{aligned} \tag{3.14}$$

It follows from Eq. (3.14) that

$$k = \frac{2(\Gamma+1)(\sigma_{32}^{\infty} + \mathrm{i}\sigma_{31}^{\infty}) - 2\bar{p}(\Gamma-1)(\sigma_{32}^{\infty} - \mathrm{i}\sigma_{31}^{\infty})}{\mu_2[(\Gamma+1)^2 - |p|^2(\Gamma-1)^2]}, \tag{3.15}$$

$$\frac{q_2}{q_1} = \frac{\overline{\xi_1^2\omega'(\xi_1)}}{\xi_2^2\omega'(\xi_2)}, \tag{3.16}$$

$$\varepsilon_{32}^* + \mathrm{i}\varepsilon_{31}^* = \frac{Rkq_1(\Gamma-1)(1-b^2)^2}{a^2(1+b^2)}\overline{\xi_1^2\omega'(\xi_1)}, \tag{3.17}$$

where

$$\omega'(\xi) = R\left[1 - \frac{p}{\xi^2} - \frac{q_1}{(\xi-\bar{\xi}_1^{-1})^2} - \frac{q_2}{(\xi-\bar{\xi}_2^{-1})^2}\right]. \tag{3.18}$$

Thus, it is seen from Eqs. (2.1), (3.11) and (3.15) that the internal uniform stress field inside the non-elliptical inhomogeneity is explicitly given by

$$\sigma_{32} + \mathrm{i}\sigma_{31} = \frac{2\Gamma[(\Gamma+1)(\sigma_{32}^\infty + \mathrm{i}\sigma_{31}^\infty) - \bar{p}(\Gamma-1)(\sigma_{32}^\infty - \mathrm{i}\sigma_{31}^\infty)]}{(\Gamma+1)^2 - |p|^2(\Gamma-1)^2}, \quad z \in S_1, \tag{3.19}$$

which is in fact independent of the existence of the non-circular (Booth's lemniscate) inclusion.

The parameter q_2 can be simply determined from Eq. (3.16) using the iteration method for given values of the four parameters ξ_1, ξ_2, p and q_1. Thus, the mapping function in Eq. (3.10) has been completely determined.

The two complex parameters z_1 and z_2 can be simply determined from Eq. (3.10) as follows

$$\begin{aligned} z_1 &= R\left(\xi_1 + \frac{p}{\xi_1} + \frac{q_1}{\xi_1 - \bar{\xi}_1^{-1}} + \frac{q_2}{\xi_1 - \bar{\xi}_2^{-1}}\right), \\ z_2 &= R\left(\xi_2 + \frac{p}{\xi_2} + \frac{q_1}{\xi_2 - \bar{\xi}_1^{-1}} + \frac{q_2}{\xi_2 - \bar{\xi}_2^{-1}}\right). \end{aligned} \tag{3.20}$$

A comparison of Eq. (3.20) with Eq. (3.6) leads to the following relationships

$$\begin{aligned} c &= \frac{z_1 + z_2}{2}, \\ \theta &= \arg(z_1 - z_2), \\ \frac{a\sqrt{b}}{1-b^2} &= \frac{|z_1 - z_2|}{2}, \end{aligned} \tag{3.21}$$

where z_1 and z_2 are determined by Eq. (3.20). Equation (3.21) indicates that the complex constant c and the phase angle θ in Eq. (3.3) can be uniquely determined by Eq. $(3.21)_{1,2}$ and that the two constants a and b in Eq. (3.3) should satisfy the relationship in Eq. $(3.21)_3$. Once the real constant $b\,(0 < b < 1)$ is also given, the other real constant $a(>0)$ can be uniquely determined from Eq. $(3.21)_3$. One

requirement is that the obtained inclusion-matrix interface L_2 does not intersect with the inhomogeneity-matrix interface L_1.

Substitution of Eqs. (3.15) and (3.18) into Eq. (3.17) yields

$$\frac{\mu_2(\varepsilon_{32}^*+\mathrm{i}\varepsilon_{31}^*)[(\Gamma+1)^2-|p|^2(\Gamma-1)^2]}{(\Gamma^2-1)(\sigma_{32}^\infty+\mathrm{i}\sigma_{31}^\infty)-\bar{p}(\Gamma-1)^2(\sigma_{32}^\infty-\mathrm{i}\sigma_{31}^\infty)} = \frac{2q_1R^2(1-b^2)^2}{a^2(1+b^2)}\left[\bar{\xi}_1^2-\bar{p}-\frac{\bar{q}_1|\xi_1|^4}{(1-|\xi_1|^2)^2}-\frac{\bar{q}_2\bar{\xi}_1^2}{(\bar{\xi}_1-\xi_2^{-1})^2}\right]. \tag{3.22}$$

The right-hand side of Eq. (3.22) is known. Thus Eq. (3.22) can be considered as a relationship between the eigenstrains imposed on the Booth's lemniscate inclusion and remote loading for the given shear moduli of the composite. The non-uniform stress field in the matrix can be conveniently established by substituting Eq. (3.13) into Eq. (2.1). It follows from Eqs. (2.1) and (3.12) that the stresses along the interface L_1 on the matrix side are always bounded even at the points where $\omega'(\xi)=0$. Furthermore, the analytic function $f_3(\xi)=f_3(\omega(\xi))$ characterizing the non-uniform stress field inside the Booth's lemniscate inclusion can be determined from Eq. (3.8) as follows

$$f_3(\xi)=f_2(\xi)-(\varepsilon_{32}^*+\mathrm{i}\varepsilon_{31}^*)\omega(\xi)+(\varepsilon_{32}^*-\mathrm{i}\varepsilon_{31}^*)D(\omega(\xi)). \tag{3.23}$$

In Eq. (3.23), $f_2(\xi)$ is given by Eq. (3.13) whereas the determination of $D(\omega(\xi))$ is somewhat involved since it is necessary to first determine the explicit expression of $m^{-1}(z)$ from Eq. (3.3). Fortunately, $m^{-1}(z)$ can indeed be determined explicitly. However, its specific expression is suppressed here for brevity.

If the eigenstrains imposed on the inclusion are zero, we have from Eq. (3.17) or (3.22) that $q_1=0$. It is then seen from Eq. (3.16) that $q_2=0$. Both parameters q_1 and q_2 taking the value zero in Eq. (3.10) means that the inhomogeneity is of elliptical shape. Thus, the non-elliptical shape of the inhomogeneity is caused solely by the presence of Booth's lemniscate inclusion.

In the following section, illustrative numerical examples is presented to demonstrate the feasibility of the general solution method proposed in this section.

4. Numerical examples

In the first example, we choose

$$\xi_1=1.5, \quad \xi_2=2.5, \quad p=0.5, \quad q_1=-0.3. \tag{4.1}$$

The parameter q_2 can be determined from Eq. (3.16) through iteration as

$$q_2=-0.1374. \tag{4.2}$$

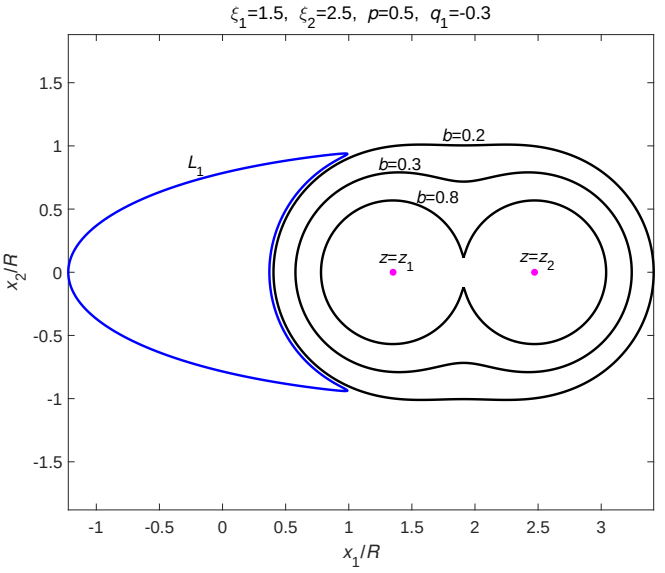

FIG. 3. The non-elliptical shape of L_1 and Booth's lemniscate shapes of L_2 for different values of b with the four parameters ξ_1, ξ_2, p and q_1 given by Eq. (4.1).

The non-elliptical shape of the inhomogeneity together with the two points $z = z_1$ and $z = z_2$ is illustrated in Fig. 3. Using Eq. (3.21), we have

$$c = 1.9097R, \quad \theta = \pi, \quad \frac{a\sqrt{b}}{1-b^2} = 0.5612R, \tag{4.3}$$

and the shapes of L_2 describing Booth's lemniscate for different values of the parameter b are also illustrated in Fig. 3. It is quite clear from Fig. 3 that the right portion of L_1 becomes non-convex due to the presence of the nearby Booth's lemniscate inclusion.

In the second example, we choose

$$\xi_1 = 3, \quad \xi_2 = 5, \quad p = 0.5, \quad q_1 = 0.15. \tag{4.4}$$

The parameter q_2 can be determined from Eq. (3.16) through iteration as

$$q_2 = 0.0510. \tag{4.5}$$

The non-elliptical shape of the inhomogeneity together with the two points $z = z_1$ and $z = z_2$ is illustrated in Fig. 4. Using Eq. (3.21), we have

$$c = 4.1919R, \quad \theta = \pi, \quad \frac{a\sqrt{b}}{1-b^2} = 0.9508R, \tag{4.6}$$

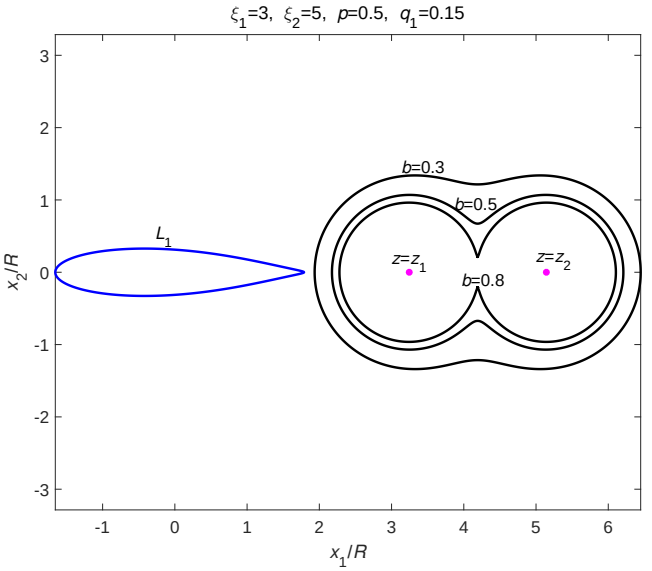

FIG. 4. The non-elliptical shape of L_1 and Booth's lemniscate shapes of L_2 for different values of b with the four parameters ξ_1, ξ_2, p and q_1 given by Eq. (4.4).

and the shapes of L_2 again describing Booth's lemniscate for different values of the parameter b are also illustrated in Fig. 4. We see from Fig. 4 that a rounded corner appears on the right portion of L_1 due to the presence of the nearby Booth's lemniscate inclusion.

In the third example, we choose

$$\xi_1 = 1.5, \quad \xi_2 = 2.5 + 0.3\mathrm{i}, \quad p = 0.5, \quad q_1 = -0.3. \tag{4.7}$$

The parameter q_2 can be determined from Eq. (3.16) through iteration as

$$q_2 = -0.1324 - 0.0275\mathrm{i}. \tag{4.8}$$

The non-elliptical shape of the inhomogeneity together with the two points $z = z_1$ and $z = z_2$ is illustrated in Fig. 5. By using Eq. (3.21), we have

$$c = (1.9146 + 0.1335\mathrm{i})R, \quad \theta = -2.8574, \quad \frac{a\sqrt{b}}{1-b^2} = 0.5831R, \tag{4.9}$$

and the shapes of L_2 describing Booth's lemniscate for different values of the parameter b are illustrated in Fig. 5. It is seen from Fig. 5 that some portion of L_1 almost touches some portion of L_2 and these two portions are almost identical when $b = 0.211$.

In the fourth example, we choose

$$\xi_1 = 1.5 + 0.5\mathrm{i}, \quad \xi_2 = 1.5 - 0.5\mathrm{i}, \quad p = 0.5, \quad q_1 = -0.2077 - 0.1323\mathrm{i}. \tag{4.10}$$

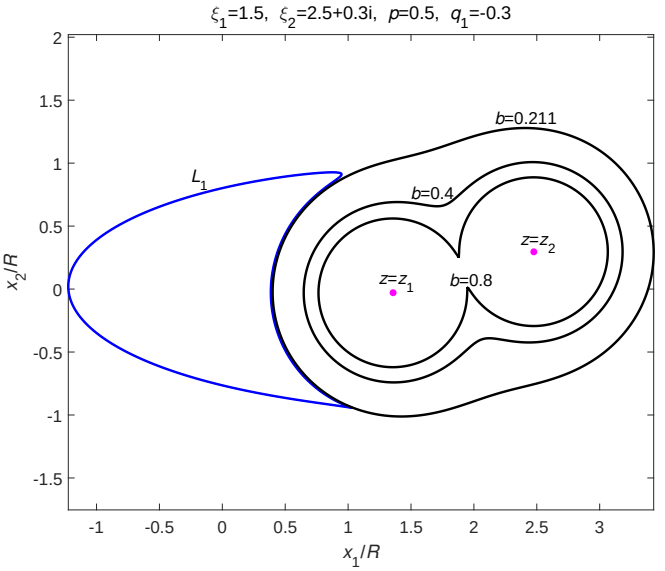

FIG. 5. The non-elliptical shape of L_1 and Booth's lemniscate shapes of L_2 for different values of b with the four parameters ξ_1, ξ_2, p and q_1 given by Eq. (4.7).

The parameter q_2 can be determined from Eq. (3.16) through iteration as

$$q_2 = \bar{q}_1 = -0.2077 + 0.1323\mathrm{i}. \tag{4.11}$$

The non-elliptical shape of the inhomogeneity together with the two points $z = z_1$ and $z = z_2$ $(= \bar{z}_1)$ is illustrated in Fig. 6. Using Eq. (3.21), we have

$$c = 1.4756R, \quad \theta = \frac{\pi}{2}, \quad \frac{a\sqrt{b}}{1-b^2} = 0.5404R, \tag{4.12}$$

and the shapes of L_2 for different values of the parameter b are also illustrated in Fig. 6. In this example, $\xi_1 = \bar{\xi}_2$, $p = \bar{p}$, and the value of the parameter q_1 is adjusted so that $q_1 = \bar{q}_2$. In doing so, both L_1 and L_2 in Fig. 6 are symmetric with respect to the x_1-axis.

In the fifth example, we choose

$$\xi_1 = 1.5, \quad \xi_2 = 2.5, \quad p = -0.5, \quad q_1 = -0.205. \tag{4.13}$$

The parameter q_2 can be determined from Eq. (3.16) through iteration as

$$q_2 = -0.1015. \tag{4.14}$$

The non-elliptical shape of the inhomogeneity together with the two points $z = z_1$ and $z = z_2$ is illustrated in Fig. 7. Using Eq. (3.21), we have

$$c = 1.4841R, \quad \theta = \pi, \quad \frac{a\sqrt{b}}{1-b^2} = 0.6557R, \tag{4.15}$$

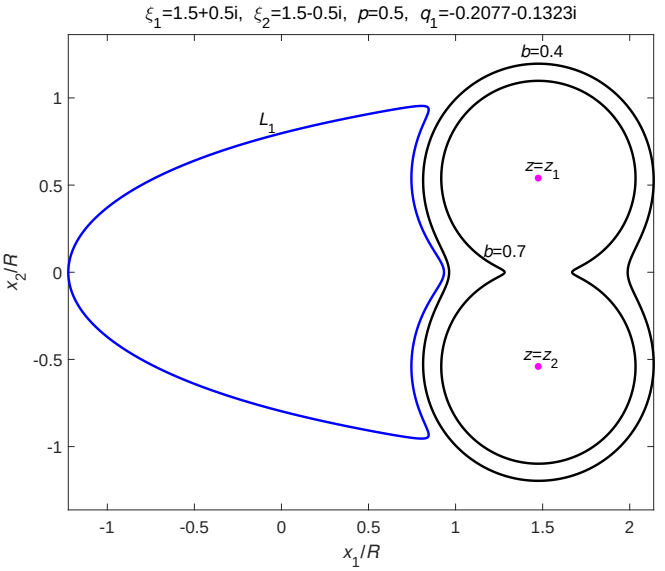

FIG. 6. The non-elliptical shape of L_1 and Booth's lemniscate shapes of L_2 for different values of b with the four parameters ξ_1, ξ_2, p and q_1 given by Eq. (4.10).

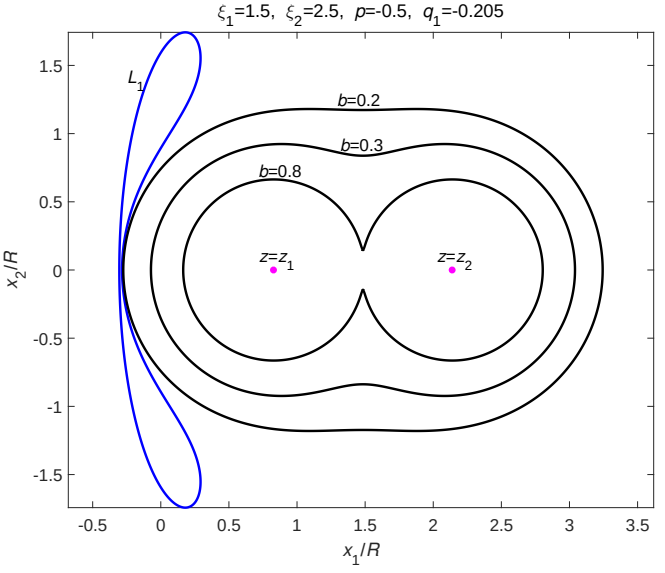

FIG. 7. The non-elliptical shape of L_1 and Booth's lemniscate shapes of L_2 for different values of b with the four parameters ξ_1, ξ_2, p and q_1 given by Eq. (4.13).

and shapes of L_2 for different values of the parameter b are also illustrated in Fig. 7. We see from Fig. 7 that: (i) one portion of L_1 almost touches another portion of L_1; (ii) L_2 almost touches L_1 when $b = 0.2$.

In the sixth and final example, we choose

$$\xi_1 = 3, \quad \xi_2 = 5, \quad p = -0.5, \quad q_1 = 0.53. \tag{4.16}$$

The parameter q_2 can be determined from Eq. (3.16) through iteration as

$$q_2 = 0.1850. \tag{4.17}$$

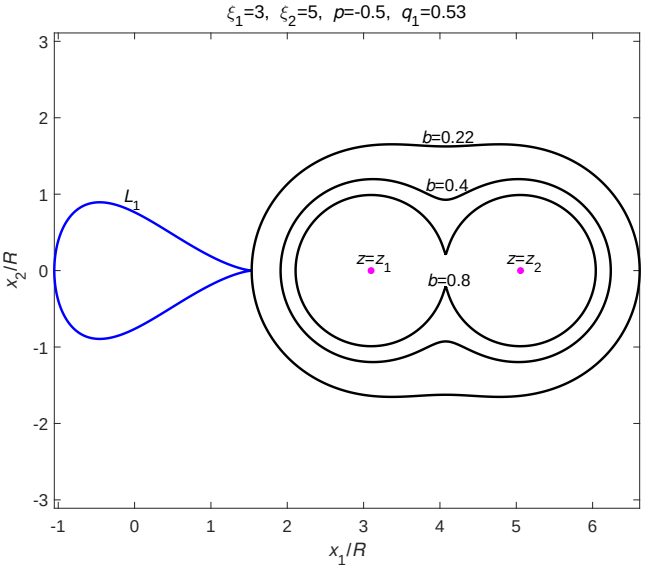

FIG. 8. The non-elliptical shape of L_1 and Booth's lemniscate shapes of L_2 for different values of b with the four parameters ξ_1, ξ_2, p and q_1 given by Eq. (4.16).

The non-elliptical shape of the inhomogeneity together with the two points $z = z_1$ and $z = z_2$ is illustrated in Fig. 8. By using Eq. (3.21), we have

$$c = 4.0751R, \quad \theta = \pi, \quad \frac{a\sqrt{b}}{1-b^2} = 0.9770R, \tag{4.18}$$

and the shapes of L_2 for different values of the parameter b are also illustrated in Fig. 8. We can see from Fig. 8 that the sharp corner of L_1 just touches L_2 when $b = 0.22$.

5. Conclusions

In this paper, we have solved the inverse problem in anti-plane elasticity associated with the uniformity of stresses inside a non-elliptical inhomogeneity interacting with a non-circular Booth's lemniscate inclusion when the matrix is

subjected to uniform remote stresses. Using analytic continuation, the analytic function $f_2(z)$ is extended to $S_2 \cup S_3$. In doing so, $f_2(z)$ has two first-order poles at $z = z_1$ and $z = z_2$ within its extended domain S_3. As a result, a conformal mapping function in Eq. (3.10) incorporating the existence of the non-circular inclusion can be introduced that maps the exterior of the inhomogeneity onto the exterior of the unit circle in the image ξ-plane. As illustrated in the numerical examples, once the four parameters ξ_1, ξ_2, p and q_1 are given, the unique non-elliptical shape of L_1 is determined and different Booth's lemniscate shapes of L_2 are permissible for different values of the parameter b as long as L_2 does not intersect with L_1 (although the two curves can 'just touch' each other). We are extremely interested in adapting the present solution method to investigate whether other non-circular shapes of the Eshelby inclusion can also induce a uniform stress field inside the non-elliptical inhomogeneity. The uniformity of stresses inside a non-elliptical inhomogeneity in the presence of both a nearby non-circular Eshelby inclusion and a nearby finite mode III crack is also an important topic for discussion. In this regard, previous studies on various crack-inhomogeneity interaction problems are abundant in the literature (see, for example, [16, 17]).

Acknowledgements

This work is supported by a Discovery Grant from the Natural Sciences and Engineering Research Council of Canada (Grant No: RGPIN–2017-03716115112).

References

1. K. Zhou, H.J. Hoh, X. Wang, L.M. Keer, J.H.L. Pang, B. Song, Q.J. Wang, *A review of recent works on inclusions*, Mechanics of Materials, **60**, 144–158, 2013.

2. M. Dai, C.F. Gao, C.Q. Ru, *Uniform stress fields inside multiple inclusions in an elastic infinite plane under plane deformation*, Proceedings of the Royal Society of London A, **471**, 2177, 20140933, 2015.

3. M. Dai, C.Q. Ru, C.F. Gao, *Uniform strain fields inside multiple inclusions in an elastic infinite plane under anti-plane shear*, Mathematics and Mechanics of Solids, **22**, 114–128, 2017.

4. X. Wang, L. Chen, P. Schiavone, *Uniformity of stresses inside a non-elliptical inhomogeneity interacting with a circular Eshelby inclusion in anti-plane shear*, Archive of Applied Mechanics, **88**, 1759–1766, 2018.

5. X. Wang, P. Schiavone, *A circular Eshelby inclusion interacting with a coated non-elliptical inhomogeneity with internal uniform stresses in anti-plane shear*, Mechanics of Materials, **128**, 59–63, 2019.

6. X. WANG, P. YANG, P. SCHIAVONE, *A circular Eshelby inclusion interacting with a non-parabolic open inhomogeneity with internal uniform anti-plane stresses*, Mathematics and Mechanics of Solids, **25**, 3, 573–581, 2020.

7. X. WANG, P. YANG, P. SCHIAVONE, *Uniform fields inside two interacting non-parabolic and non-elliptical inhomogeneities*, Journal of Applied Mathematics and Physics, **71**, 1, 25, 2020.

8. Y.A. ANTIPOV, *Method of automorphic functions for an inverse problem of antiplane elasticity*, Quarterly Journal of Mechanics and Applied Mathematics, **72**, 2, 213–234, 2019.

9. Y.A. ANTIPOV, *Method of Riemann surfaces for an inverse antiplane problem in an n-connected domain*, Complex Variables and Elliptic Equations, **65**, 455–480, 2020.

10. J.S. MARSHALL, *On sets of multiple equally strong holes in an infinite elastic plate: parameterization and existence*, SIAM Journal on Applied Mathematics, **79**, 2288–2312, 2019.

11. M. LIM, G.W. MILTON, *Inclusions of general shapes having constant field inside the core and nonelliptical neutral coated inclusions with anisotropic conductivity*, SIAM Journal on Applied Mathematics, **80**, 3, 1420–1440, 2020.

12. C.Q. RU, *Analytic solution for Eshelby's problem of an inclusion of arbitrary shape in a plane or half-plane*, ASME Journal of Applied Mechanics, **66**, 315–322, 1999.

13. H. NOZAKI, M. TAYA, *Elastic fields in a polygon-shaped inclusion with uniform eigenstrains*, ASME Journal of Applied Mechanics, **64**, 495–502, 1997.

14. H. NOZAKI, M. TAYA, *Elastic fields in a polyhedral inclusion with uniform eigenstrains and related problems*, ASME Journal of Applied Mechanics, **68**, 3, 441–452, 2001.

15. T.C.T. TING, *Anisotropic Elasticity: Theory and Applications*, Oxford University Press, New York, 1996.

16. Z.M. XIAO, H.X. ZHANG, B.J. CHEN, *Micro-crack initiation at the tip of a semi-infinite rigid line inhomogeneity in piezoelectric solids*, International Journal of Engineering Science, **43**, 1223–1233, 2005.

17. Z.M. XIAO, K.D. PAE, *The interaction between a penny-shaped crack and a spherical inhomogeneity in an infinite solid under uniaxial tension*, Acta Mechanica, **90**, 91–104, 1991.

Received July 08, 2021; revised version October 09, 2021.
Published online December 07, 2021.